Using true-amplitude MZO to improve geometrical spreading corrections for AVO

Antônio C. B. Ramos*, Adelson S. de Oliveira* and Martin Tygel**

* PETROBRAS S/A, Brazil

** State University of Campinas, UNICAMP, Brazil

Abstract

We discuss the application of true-amplitude Dip Move-Out (DMO) to amplitude versus offset (AVO) studies on real marine seismic data. Besides the usual kinematics of any DMO process, true amplitude DMO is designed to properly account for the variations in the geometrical spreading losses with offset. After the application of a true-amplitude DMO, primary reflections in the input CO section are transformed into their corresponding ZO primary reflections so that (a) geometrical spreading losses are automatically transformed and (b) reflection coefficients remain unchanged. The process effects, thus, the desired compensation of the offset-dependent, geometrical-spreading, which is needed for a reliable AVO analysis. The performance of the proposed true-amplitude DMO algorithm to correctly compensate geometrical-spreading losses at large offsets is examined. For a known gas anomaly the AVO gradient section showed larger absolute values, indicating larger amplitude compensation not predicted by conventional methods. The reliable results obtained by the proposed method have shown to be useful for AVO analysis.

INTRODUCTION

The construction of a simulated zero-offset (ZO) section out of a given constant-offset (CO) section is often referred in the seismic literature as a Migration to Zero Offset (MZO). The first task of an MZO operator is to correctly map primary reflections in the original CO section into their corresponding positions in the simulated ZO section. The MZO process is called true amplitude if, in addition to kinematical positioning, also the amplitude losses of primary reflections due to geometrical spreading are correctly accounted for. Under fairly general laterally inhomogeneous background media, true-amplitude, Kirchhoff-type, weighted stacking schemes have been described in Tygel et al. (1998). For the case of a homogeneous background, a comprehensive description of MZO (also called transformation to zero offset) can be found in Bleistein (1999). As shown below, true-amplitude DMO may be particularly advantageous when applied to input CO sections where no previous geometrical-spreading corrections have been applied. In this case, the geometrical-spreading losses in the amplitudes of primary reflections after true-amplitude DMO should be the same as the ones obtained if an actual ZO experiment were actually performed. A comprehensive discussion on the amplitude results of various MZO algorithms is presented in Tygel et al. (1998).

It is to be observed that all other factors that affect the amplitude of primary reflections are not affected by the application of true-amplitude MZO. This includes, e.g., losses due to reflection at the target reflector, transmission across interfaces and attenuation along the ray paths. For AVO purposes, it is fortunate that the offset-dependent CO primary reflections remain unchanged after the application of a true-amplitude MZO. Apart from geometrical spreading, reflection coefficients are, in most situations, the quantities that most influence primary-reflection amplitudes. In most applications, other wave-propagation effects like, e.g., attenuation and transmission losses across interfaces, present lesser lateral variation, being simply taken as scaling factors in AVO studies. As true-amplitude MZO reduces original CO geometrical-spreading factors to their fixed ZO counterpart, this quantity also becomes a scaling factor in the primary-reflection output amplitudes. As a consequence, these resulting amplitudes become a measure of the reflection-coefficient variation with offset, which is the aim of AVO analysis.

In areas with moderate geological complexity, true-amplitude MZO is usually obtained via standard NMO followed by true-amplitude DMO. True-amplitude DMO algorithms can be directly derived by their counterpart MZO algorithms. Moreover, the stacking curves and weight functions reduce to simple, analytic expressions, leading to fast and efficient algorithms. Applications of true-amplitude DMO to real-data imaging are reported, e.g., in Oliveira et al. (1997). Similar to what has been explained before for the case of MZO, if no geometrical-spreading corrections are previously applied, true-amplitude DMO transforms a CO section into simulated ZO section for which primary reflections possess the same geometrical-spreading factor as would be observed in a direct ZO experiment. At the same time, reflection coefficients remain the same as in a CO experiment. As a consequence, amplitudes obtained from the application of true-amplitude DMO to several CO sections can be seen as essentially the offset-dependent reflection coefficients scaled by a constant ZO geometrical-spreading factor. As the latter can be reasonably estimated by NMO velocities, true-amplitude DMO is expected to provide more reliable amplitudes, better compensated for offset-dependent geometrical-spreading factors, more suitable for AVO studies. Our purpose here is to investigate on a specific real data example and in the framework

of AVO analysis, the application of a true-amplitude DMO, as compared with a more conventional one used in practice.

BASIC THEORY OF THE TRUE-AMPLITUDE DMO

The new DMO has the same well-known kinematics of the standard processes. It is implemented in the space-time domain via Kirchhoff summation along a prescribed integration path with weights that insure a true-amplitude result in the sense above. For an input CO section $U(\xi,t)$ consisting of NMO corrected analytic traces, the corresponding simulated ZO section $V_0(\xi_0,t_0)$ can be obtained (Oliveira et al., 1997; Tygel et al. 1998) by

$$V(\xi_0,t_0)=\frac{1}{\sqrt{2\pi}}\int_A d\xi\ K(\xi;\xi_0,t_0)\ D_-^{1/2}\ U(\xi,t)\ \Big|_{t=\tau(\xi;\xi_0,t_0)}\ , \tag{1}$$

where (ξ,t) and (ξ_0,t_0) stands for the input CO mid-point and time coordinates and the location and time coordinates of the ZO section, respectively. $D^{1/2}$ is the anti-causal half derivative defined by,

$$D_-^{1/2}\ U(\xi,t)=\frac{1}{2\pi}\int_{-\infty}^{\infty} d\omega\ e^{i\omega t}|\omega|^{1/2}\ e^{i\frac{\pi}{4}\mathrm{sgn}(\omega)}\ \hat{U}(\xi,\omega)\ , \tag{2}$$

with

$$U(\xi,\omega)=\int_{-\infty}^{\infty} dt\ e^{-i\omega t}\ U(\xi,t). \tag{3}$$

Expressions for the stacking curve and the weight function, depending on dynamic ray tracing computed on an an arbitrary, laterally inhomogeneous macro-velocity model are derived in Tygel et al. (1998). For a constant-velocity background, these reduce to simple analytic formulas. Introducing the convenient notation $\eta=(\xi-\xi_O)/h$, where h is the half offset, the stacking curve can be written

$$t=\tau_{DMO}(\xi;\xi_0,t_0)=\frac{t_0}{\sqrt{1-\eta^2}}\ , \tag{4}$$

the weight function being

$$K(\xi;\xi_0,t_0)\ =\ \frac{2}{v\sqrt{t_0}}\sqrt{1+\frac{(vt_0/2h)^2}{1-\eta^2}}\,\frac{1+\eta^2}{(1-\eta^2)^{3/2}}\ . \tag{5}$$

As shown in Bleistein et al. (1999), aperture A in equation (1) can be restricted to those midpoints that collect non-evanescent energy only. This is guaranteed if we set

$$\eta<\sqrt{1+\left(\frac{v\,t_0}{4h}\right)^2}-\frac{v\,t_0}{4h}\ . \tag{6}$$

At least for areas of mild velocity variations, it is reasonable to still apply the simple expressions above, upon replacing the constant velocity value *v* in equation (5) by the NMO velocity at the point where the ZO section is to be simulated.

APPLICATION TO REAL DATA

To best illustrate the benefits true-amplitude DMO can bring to AVO analysis, we compare the amplitude responses of a real dataset as a result of two processing alternatives. These are (a) conventional offset-dependent geometrical-spreading correction, followed by the application of F-K DMO and (b) direct applicaton of true-amplitude DMO, followed by ZO geometrical-spreading correction. The dataset is characterized by a strong AVO anomaly, related to a thick tertiary sandstone reservoir saturated by methane gas and embedded in marine shales (Ramos et al., 1998). Figures 1 and 2 show the AVO gradient sections obtained for the two processing alternatives on the given dataset, respectively. The amplitude anomaly at the top of the sandstone reservoir is shown by the strong trough at 2.4 s. A flat spot appears at the base of the reservoir indicating the water/gas contact. The data processed with F-K DMO shows overall smaller amplitudes than the data processed with true-amplitude DMO. Additionally, the true-amplitude DMO case shows a significant improvement in the amplitude ratio between the anomalous zones and the background reflections throughout the entire section. Figure 3 shows the amplitude versus offset comparison for the top of the reservoir (2.35-2.40 s) using standard F-K DMO and true-amplitude DMO. The latter shows larger amplitudes in far offsets, which produced larger AVO gradients. Figure 4 shows the gradient values at the top of the reservoir for a range of 25 CMPs. The AVO gradient is consistently larger for the true-amplitude DMO case throughout the entire extent of the reservoir. For events with small dip, standard F-K DMO does not introduce appreciable variations throughout the input amplitude spectrum. Therefore, this process should not change significantly the AVO gradient. As a consequence, the significant differences in the far-offset amplitudes introduced by the application of true-amplitude DMO process may be due to the different geometrical-spreading compensation in both processes.

To provide a more quantitative justification of the above claim, we take a closer look at the actual expressions used in practice to approximate offset-dependent geometrical spreading. Ursin (1990) provides a comprehensive analysis of these expressions. All of them are obtained in the form of truncated power series expansions on offset, of exact formulas for plane-stratified media. They are thus expected to provide accurate results in the near-offset range. This is confirmed in Ursin (1990) upon the use of synthetic examples. An interesting result of Ursin's experiments is that, as offsets get larger, all approximation formulas increasingly underestimate the corresponding exact value. This means that geometrical-spreading correction using these approximations will, at least in the case of a plane-stratified model, produce smaller amplitudes. Very reasonably, this general trend is to be expected to hold also in more general situations. In the present case, the comparisons on AVO and amplitude gradient shown in Figures 3 and 4, respectively, are consistant with the expected behavior, as predicted in Ursin (1990). Conventional corrections based on underestimated offset-dependent geometrical-spreading factors in FK DMO, lead to smaller amplitudes and gradients as compared to their counterparts obtaind after true-amplitude DMO.

To better correlate amplitude with lithology and fluids it is important to observe the AVO data in terms of gradient versus intercept crossplots. This methodology has been extensively discussed in the literature (see, e.g., Verm and Hilterman, 1995 and Ramos, 1998) and it has become an important tool for definition of the background trend, which is dominated by water sands and shales, and for classification of anomaly types. This classification strongly relies on the spatial position of the anomaly with respect to horizontal (intercept) and vertical (gradient) axes and the background trend, which is defined by a line fit through the origin in the gradient- versus-intercept graph. Non-pay lithologies (shales and water sands) tend to align along or closer to the background trend, whereas pay zones associated with bright-spots sands, for example, tend to deviate from the background trend. The seismic background trend is calibrated with the similar trend derived from well logs. The target anomaly shown in Figures 1 and 2 is a typical bright spot caused by the presence of gas in high porosity sands encased by marine shales. In terms of gradient-versus-intercept crossplot, these anomalous amplitudes are distributed in the first and third quadrants. Figures 5 and 6 show the crossplot gradient versus intercept for the seismic data processed with F-K DMO and true-amplitude DMO. Crossplot values were selected from a time window including the anomaly associated with the gas reservoir. The background trend is reasonably defined in both figures, but there is a considerable difference in the departure from this line for the anomalous amplitudes in the first and third quadrants. In the FK-DMO case, a considerably smaller scatter of the amplitudes around the background trend is observed. This smaller scatter is caused by the poor gradient estimation, particularly for long offsets and dipping events, associated with the processing sequence involving offset-dependent geometrical spreading followed by F-K DMO. The crossplot for the true-amplitude DMO case (Figure 6) shows a significantly larger scatter and better separation of the anomalous values in the first and third quadrants, when compared with the F-K DMO case (Figure 5). This can be interpreted by the fact that the gradients are better estimated using the true-amplitude DMO processing sequence, due to more accurate geometrical-spreading compensation of amplitudes at far offsets.

CONCLUSIONS

This work has demonstrated the value of true-amplitude DMO to improve AVO analysis in the presence of dip. True-amplitude DMO shares the benefits, common to all DMO schemes, of reducing the amplitude mix caused by smearing and mispositioning of reflection points. The main advantage of true-amplitude DMO, as compared to more tradional methods, lies in its ability to perform a better compensation of geometrical-spreading losses with offset. To evaluate the potential of true-amplitude DMO as a means to improve AVO, we have considered its application on a real dataset example including an AVO anomaly. The more reliable amplitudes obtained upon the application of true-amplitude DMO, made possible a better estimation of AVO attributes such as AVO gradient. It has further contributed to better delineate and enhance the AVO anomaly.

REFERENCES

*Fomel, S., Bleistein, N., Cohen, J. K. and Jaramillo, H., 1998, True-amplitude transformation to zero offset of data from curved reflectors: Geophysics, **64**, 112-129.*

*Oliveira, A. S., Tygel, M., and Filpo, E., 1997, On the application of true-amplitude DMO, J. Seism. Expl., **6**, 279-289.*

*Ramos, A. C. B., 1998, AVO Processing Calibration, The Leading Edge, **17**, n.8, 1075-1082.*

Ramos, A. C. B, Guimarães, S. O. and Silva, S. R. P., 1998, Foz do Amazonas Basin: A classical example of successful aplication of AVO technology, AAPG Intl. Conf. and Exhibition, Rio de Janeiro, Brazil.

*Tygel, M., Schleicher, J., Hubral, P,, and Santos, L. T., 1998, 2.5-D true-amplitude Kirchhoff migration to zero offset in laterally inhomogeneous media: Geophysics, **63**, 557-573.*

*Ursin, B., 1990, Offset dependent geometrical spreading in layered medium, Geophysics, **55**, n.4, 492-496.*

*Verm, R., and Hilterman, F., 1995, Lithology color-coded sections: The calibration of AVO crossplotting to rock properties, The Leading Edge, **14**, n.8, 847-853.*

ACKNOWLEDGMENTS

We thank PETROBRAS SA for the permission to publish this work.

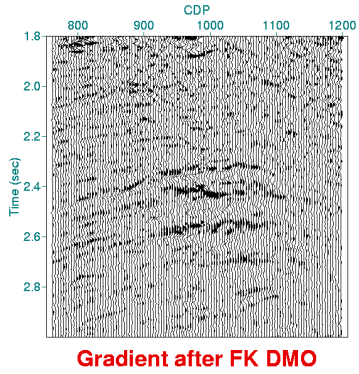

Figure 1 – AVO gradient section of a known gas sand anomaly obtained after preprocessing with F-K DMO. Notice the negative gradient at 2.4 s associated with the top of the reservoir.

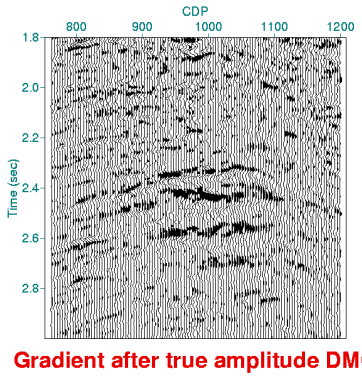

Figure 2 - AVO gradient section of the same anomaly, obtained after preprocessing with true-amplitude DMO. Notice the improved amplitude ratio between the anomaly and the background reflections, as compared to Figure 1.

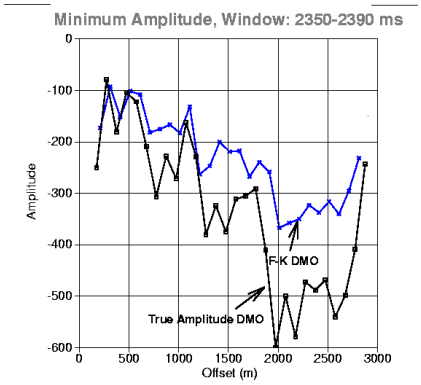

Figure 3 – Amplitude versus offset comparison between traditional (F-K) DMO and true-amplitude DMO for a window at the top of the reservoir. Offset-dependent, geometrical spreading was applied to the data before F-K DMO.

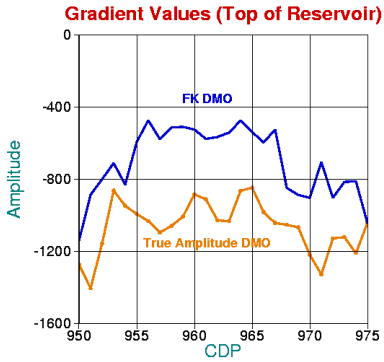

Figure 4 – AVO gradient values at the top of the reservoir. Notice that gradient values are consistantly higher for the true-amplitude DMO case.

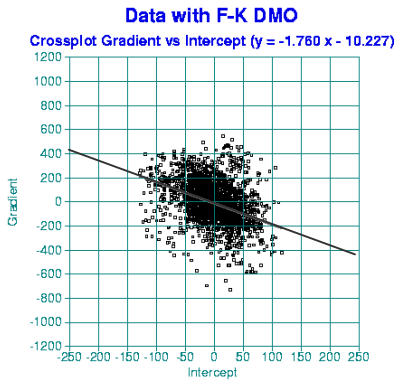

Figure 5 - Crossplot of AVO gradient versus AVO intercept for the data processed with F-K DMO. Crossplot values were selected from a window, which includes the gas anomaly shown in Figures 1 through 3.

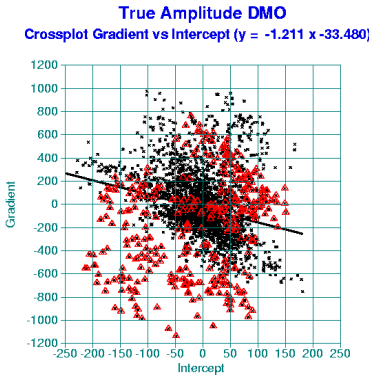

Figure 6 – Crossplot of AVO gradient versus AVO intercept for the data processed with true amplitude DMP. Crossplot values are from a window including shales (shown by x's) and the sand in the target zone (shown by triangles). Notice the better separation of the anomalous values.